Thermoelectric Effects in Nanowire-Based MOSFETs

Riccardo Bosisio, Geneviève Fleury, Cosimo Gorini, J.-L Pichard

Thermoelectric Effects in Nanowire-Based MOSFETs

Riccardo Bosisio[1], Geneviève Fleury[1], Cosimo Gorini[1,2] and Jean-Louis Pichard[1**]

[1] SPEC, CEA, CNRS, Université Paris-Saclay, CEA-Saclay, 91191 Gif-sur-Yvette, France

[2] Institut für Theoretische Physik, Universität Regensburg, 93040 Regensburg, Germany

July 3, 2017

Abstract

We review a series of works describing thermoelectric effects in gated disordered nanowires (field effect transistor device configuration). After considering the elastic coherent regime characterizing sub-Kelvin temperatures, we study the inelastic activated regime occurring at higher temperatures, where electronic transport is dominated by phonon-assisted hops between localised states (Mott variable range hopping). The thermoelectric effects are studied as a function of the location of the Fermi level inside the nanowire conduction band, notably around its edges where they become very large. We underline the interest of using electron-phonon coupling around the band edges of large arrays of parallel nanowires for energy harvesting and hot spot cooling at small scales. Multiterminal thermoelectric transport and ratchet effects are eventually considered in the activated regime.

1 Introduction

Let us consider a nanowire (NW) connecting two electron reservoirs. If one imposes a temperature difference δT between the reservoirs, this induces an electrical current I_e which can be suppressed by a voltage difference $-\delta V$. The ratio $S = -(\delta V/\delta T)_{I_e=0}$ defines the NW Seebeck coefficient (or thermopower). If one imposes a voltage difference δV when $\delta T = 0$, this induces electrical and heat currents I_e and I_Q. The ratio $\Pi = I_Q/I_e$ defines the NW Peltier coefficient. In the linear response regime, the Peltier and Seebeck coefficients are related via the Kelvin-Onsager relation $\Pi = ST$.

Either a temperature gradient across a NW can produce electricity (Seebeck effect), or an electric current through the same NW can create a temperature difference between its two sides (Peltier effect). These thermoelectric effects (TEs) can be used either for harvesting electrical energy from wasted heat or for cooling things. Today, the batteries of our cell phones and laptops need to be charged too often. Tomorrow, the Seebeck effect could allow us to exploit the wasted heat to produce a part of the electrical energy necessary for many devices used for the internet of things. Another important issue is cooling, notably the hot spots in microprocessors. The last decades have been characterized by an exponential growth of the on-chip power densities. Values of the order of $100W/cm^2$ have become common [1]. More than our ability to reduce their sizes, the limitation of the performances of microprocessors comes from the difficulty of managing heat in ever-smaller integrated circuits. Improving Peltier cooling and heat management from the nanoscale (e.g. molecules) to the microscale (e.g. quantum dots and nanowire arrays) is thus of paramount importance to boost microprocessors' performance.

In a typical two-terminal configuration in which a device is coupled to two electronic reservoirs held at different temperatures, the ratio η of the output power over the heat extracted from the hot reservoir measures the efficiency of the heat-to-work thermoelectric conversion. It cannot exceed the Carnot efficiency $\eta_C = 1 - T_C/T_H$, where T_C (T_H) is the temperature of the cold (hot) reservoir. The figure of merit ZT gives the maximal efficiency η_{max} in terms of the Carnot limit [2, 3].

$$ZT = \frac{GS^2}{K^e + K^{ph}}T; \qquad \eta_{max} = \eta_C \frac{\sqrt{ZT+1}-1}{\sqrt{ZT+1}+1}, \tag{1}$$

**Corresponding author. Email: jean-louis.pichard@cea.fr

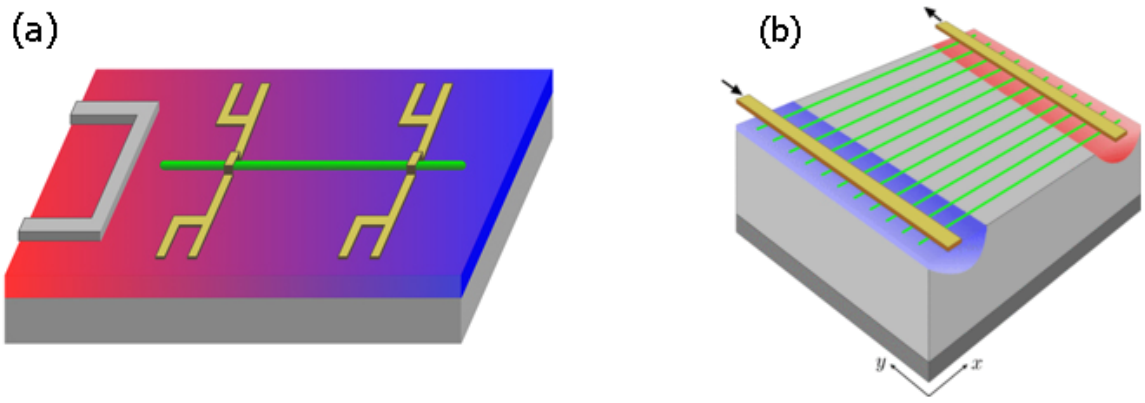

Figure 1: NW-based MOSFETs: (**a**) A single NW (green) is deposited on an insulating substrate (red and blue). The source and the drain are made of two metallic electrodes (yellow), while Joule heating from an extra electrode (left side) can induce a temperature difference between the NW extremities. Varying the voltage V_g applied upon the back gate (grey), one can shift the NW conduction band and probe thermoelectric transport in the bulk of the band, around its edges or even outside the band. This setup has been used in Ref. [12] for measuring the thermopower $\mathcal{S}$ of individual Si and Ge/Si NWs as a function of V_g at room temperature. (**b**) Array of parallel NWs deposited on a substrate with a back gate. The blue and red spots illustrate local cooling and heating effects in the activated regime, discussed in Sec.4.

where G is the electrical conductance, while K^e and K^{ph} are respectively the electronic and phononic parts of the thermal conductance. The larger ZT, the better the efficiency. A high efficiency is however mainly useful if coupled with good electrical output power, measured by the power factor $Q = GS^2$. Maximising both ZT and Q is the central challenge of (linear response) thermoelectricity. This is not easy since G, K_e, K_{ph} and S are not independent.

The interest of NWs for thermoelectric conversion was pointed out in Ref. [4]. Taking arrays of parallel doped Si NWs of 50 nm in diameter yields $ZT = 0.6$ at room temperature, a much larger value than in bulk silicon. This was attributed to a 100-fold reduction in thermal conductivity, assuming than S and G keep the same values than in doped bulk Si. Using standard Si-based semiconductor technology for thermoelectric conversion looks very interesting: In contrast to used thermoelectric materials, Si is cheap and non toxic, and NW-based one dimensional (1D) electronics is a well developed technology. Moreover, one can use metallic gates for tuning the NW electron density, in the field effect transistor (FET) device configuration. A detailed experimental study of electron tunneling and interferences in 1D Si-doped Ga-As MOSFETs can be found in Ref. [5], where the electrical conductance G of $1\mu m$ long NWs at $35mK$ is given as a function of the gate voltage V_g. One can make [6] arrays of vertical NW-based FET, each of them having a uniform wrap-around gate. To grow millions of thin NWs per cm^2 is possible. This gave us the motivation to study the TEs in 1D MOSFETs, from cryogenic temperatures where electron transport remains coherent towards higher temperatures where transport becomes activated, as a function of the location of the Fermi potential E_F inside the NW conduction band. The considered setups are sketched in Fig. 1.

There are many highly cited works describing the thermoelectric performance of NWs made of different materials: rough silicon [4, 7], bismuth [8], bismuth telluride, III-V semiconductors (InP, InAs, and GaAs) [9], wide band gap semiconductors (ZnO and GaN) [10]. These studies have essentially been done around room temperature, and are mainly focused on the study of the phononic contribution to the thermal conductance [4, 7] or of the effect of channel openings occuring when one varies the widths of superlattice quasi-1D NWs [8, 11]. Thermoelectric transport is often described using 1D Boltzmann equations [9, 8, 10], and the role of localised impurity states (important in weakly doped semiconductors) as well as the Anderson localisation of the states (important in the 1D-limit) is not taken into account in these studies.

In this short review, we describe the effect of 1D Anderson localisation upon 1D thermoelectric transport, as one varies the location of the Fermi potential E_F inside the NW conduction band. For this

purpose, we use a purely 1D model (1D Anderson model) where the energy dependence of the localisation length and of the density of states is analytically known in the weak disorder limit. Though it does not allow us to describe the effect of channel openings occuring as one varies the NW width as in Refs. [8, 11], these studies describe thermoelectric transport in NWs where the one body states are localised. A low temperature elastic regime is considered where the conductance and the thermopower are respectively obtained from the Landauer and Mott formulas, followed by the study of an inelastic regime occuring at higher temperatures and characterised by phonon-activated hopping between localised states (Mott variable range hopping). In this activated regime, thermoelectric transport is not described using semi-classical Boltzmann equations, but from the numerical solution of the random resistor network model introduced by Miller and Abrahams for describing inelastic activated transport.

2 Elastic thermoelectric transport

To model a gated NW, we have considered in Ref. [13] a chain of N sites coupled to two electronic reservoirs L (left) and R (right), in equilibrium at temperature $T_L = T + \delta T$ [$T_R = T$] and chemical potential $\mu_L = E_F + \delta\mu$ [$\mu_R = E_F$]. The Hamiltonian of the chain reads

$$\mathcal{H} = -t \sum_{i=1}^{N-1} \left(c_i^\dagger c_{i+1} + \text{h.c.} \right) + \sum_{i=1}^{N} (\epsilon_i + V_g) c_i^\dagger c_i \,, \tag{2}$$

where $c_i^\dagger$ and c_i are the creation and annihilation operators of one electron on site i and t is the hopping energy. The lattice spacing $a = 1$, the ϵ_i are (uncorrelated) random numbers uniformly distributed in the interval $[-W/2, W/2]$. $\sum_i V_g c_i^\dagger c_i$ describes the effect of an external gate. Varying V_g, one can probe thermoelectric transport either in the bulk of the NW conduction band, around its edges or even outside the band.

2.1 Typical thermopower

For the Hamiltonian (2), the localisation length $\xi(E)$ and the density of states (DOS) $\nu(E)$ per site are analytically known [14] in the weak disorder limit $W \leq t$. Within the band ($|E - V_g| \lesssim 1.5t$), $\xi(E)^{-1}$ can be expanded in integer powers of W while $\nu(E)$ remains well described by the DOS of the clean chain ($W = 0$). This gives the bulk expressions

$$\xi_b(E) \approx \frac{24}{W^2} \left(4t^2 - |E - V_g|^2 \right), \qquad \nu_b(E) \approx \frac{1}{2\pi t \sqrt{1 - (|E - V_g|/2t)^2}}. \tag{3}$$

When $E - V_g$ approaches the band edges $\pm 2t$, these expressions lead to divergences of ν and ξ^{-1}. As shown by Derrida and Gardner, these divergences are spurious and the correct expressions near the edges become

$$\xi_e(E) = 2 \left(\frac{12t^2}{W^2} \right)^{1/3} \frac{\mathcal{I}_{-1}(X)}{\mathcal{I}_1(X)} \tag{4}$$

$$\nu_e(E) = \sqrt{\frac{2}{\pi}} \left(\frac{12}{tW^2} \right)^{1/3} \frac{\mathcal{I}_1(X)}{[\mathcal{I}_{-1}(X)]^2} \tag{5}$$

where

$$X = (|E - V_g| - 2t) t^{1/3} (\frac{12}{W^2})^{2/3}, \qquad \mathcal{I}_n(X) = \int_0^\infty y^{n/2} \, e^{-\frac{1}{6}y^3 + 2Xy} \, dy \,. \tag{6}$$

The transmission coefficient $\mathcal{T}(E)$ of the disordered chain behaves typically as $\exp -2N/\xi(E)$. In the low temperature limit $T \to 0$, the electrical conductance $G \approx \frac{2e^2}{h} \mathcal{T}(E_F)$ while the thermopower S is given by the Cutler-Mott formula,

$$S = \frac{\pi^2 k_B^2 T}{3|e|t} \mathcal{S} \quad \text{with} \quad \mathcal{S} \approx -t \left. \frac{\mathrm{d} \ln \mathcal{T}}{\mathrm{d}E} \right|_{E_F} . \tag{7}$$

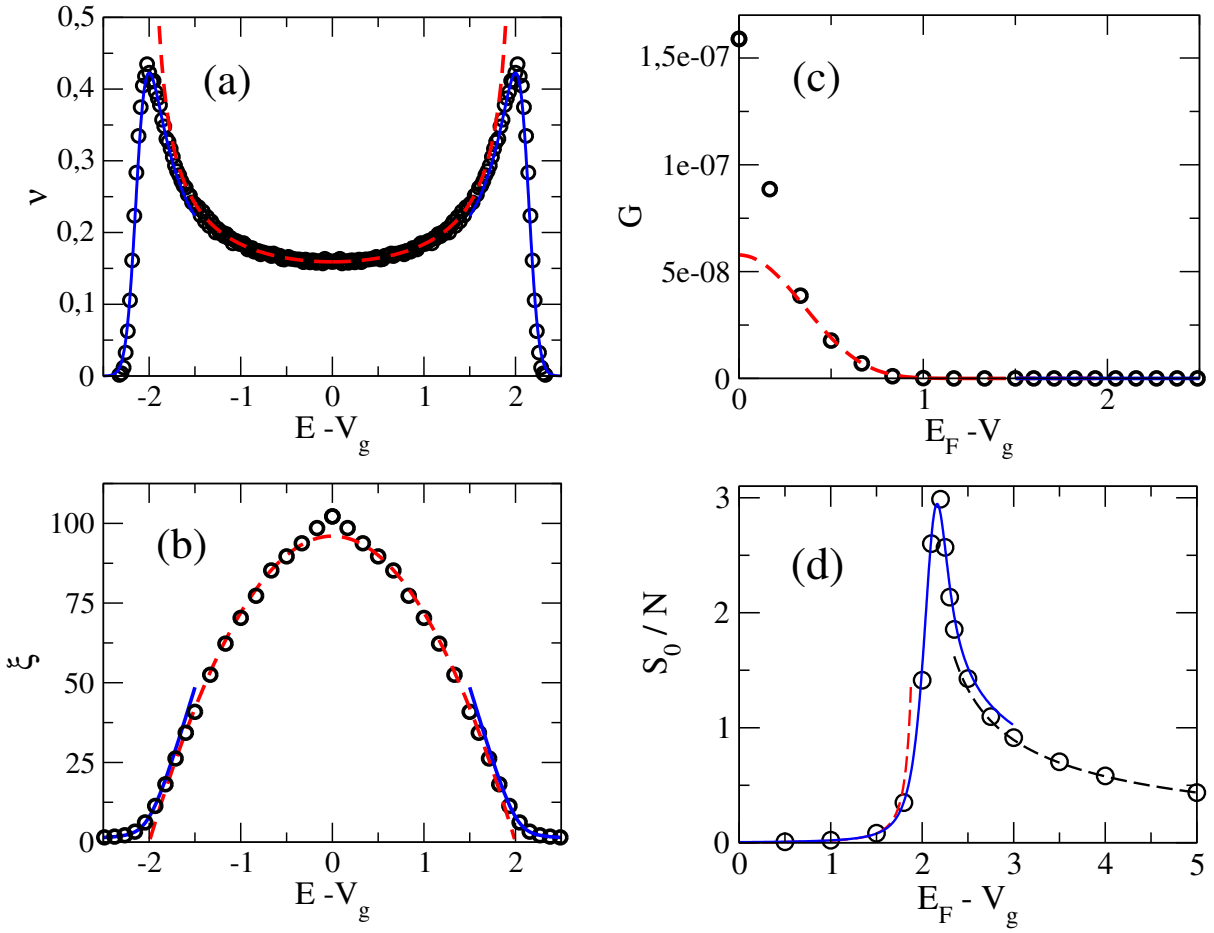

Figure 2: 1D Anderson model with $W = t = 1$: (**a**) Density of states per site $\nu(E)$, (**b**) localisation length $\xi(E)$, (**c**) typical conductance G (in units of $2e^2/h$) and (**d**) typical thermopower S_0 (in units of $(\pi^2 k_B)/(3e)\, k_B T$). In all panels, the red dashed line and the blue continuous line give the weak disorder behaviours in the bulk and near the edges (Eqs. (3-5) and Eqs. (8-9)), while the black dashed line in (d) corresponds to Eq. (10). Circles are numerical results obtained for $N = 1600$ ((a) and (b)) and $N = 800$ ((c) and (d)).

From the weak disorder expansions of $\xi(E)$, one can deduce the typical dimensionless thermopower $\mathcal{S}_0$ (thermopower in units of $(\pi^2 k_B^2 T)/(3|e|t)$). This gives respectively in the bulk of the band (superscript b) and at its edges (superscript e):

$$\mathcal{S}_0^b = N \frac{(E_F - V_g)\, W^2}{96 t^3 [1 - ((E_F - V_g)/2t)^2]^2}, \tag{8}$$

$$\mathcal{S}_0^e = 2N \left(\frac{12t^2}{W^2}\right)^{1/3} \left\{ \frac{\mathcal{I}_3(X)}{\mathcal{I}_{-1}(X)} - \left[\frac{\mathcal{I}_1(X)}{\mathcal{I}_{-1}(X)}\right]^2 \right\}, \tag{9}$$

where $X = X(E = E_F)$. Outside the band, one estimates the typical thermopower by assuming that the system behaves as a clean tunnel barrier (superscript TB). One obtains

$$\frac{\mathcal{S}_0^{TB}}{N} \underset{N\to\infty}{\approx} -\frac{1}{N} \frac{2t}{\Gamma(E_F)} \left.\frac{\mathrm{d}\Gamma}{\mathrm{d}E}\right|_{E_F} \mp \frac{1}{\sqrt{\left(\frac{E_F - V_g}{2t}\right)^2 - 1}} \tag{10}$$

with a + sign when $E_F \leq V_g - 2t$ and a − sign when $E_F \geq V_g + 2t$. Here $\Gamma(E) = i[\Sigma(E) - \Sigma^\dagger(E)]$ where $\Sigma(E)$ is the self-energy of the (identical) left and right leads, evaluated at the sites located at the chain extremities to which the leads are attached. In Fig. 2, one can see that the analytical weak disorder expressions of the DOS per site $\nu(E)$, of the localisation length $\xi(E)$, of the electrical conductance $G(E_F)$ and of the typical thermopower $S_0(E_F)$ (in units of $(\pi^2 k_B^2 T)/(3|e|t)$) describe accurately numerical results (for more details, see Ref. [13]), even if they are computed for a relatively large disorder ($W = t$).

2.2 Mesoscopic Fluctuations

In the elastic localized regime, the sample-to-sample fluctuations of the dimensionless thermopower $\mathcal{S}$ around its typical values $\mathcal{S}_0^b$ or $\mathcal{S}_0^e$ turn out to be large. If $E_F = V_g$, $\mathcal{S}_0 = 0$ due to particle-hole symmetry but the mesoscopic fluctuations allow for a large $\mathcal{S}$ anyway. Assuming Poisson statistics for the energy levels, Van Langen *et al* showed in Ref. [15] that the thermopower distribution is a Lorentzian when $N \gg \xi$,

$$P(\mathcal{S}) = \frac{1}{\pi} \frac{\Lambda}{\Lambda^2 + (\mathcal{S} - \mathcal{S}_0)^2}\,. \tag{11}$$

The width $\Lambda = 2\pi t/\Delta_F$ is given by the mean level spacing $\Delta_F = 1/(N\nu(E_F))$ at the Fermi energy E_F. Van Langen *et al* assumed $\mathcal{S}_0 = 0$, an assumption which is only correct at the band centre. We have calculated $P(\mathcal{S})$ using recursive Green function method for different values of V_g and have numerically checked [13] that Eq. (11) describes also $P(\mathcal{S})$ if one takes for $\mathcal{S}_0$ the value given by Eqs. (8) or (9) instead of $\mathcal{S}_0 = 0$. As one crosses the band edges, we have numerically observed a sharp crossover towards a Gaussian distribution

$$P(\mathcal{S}) = \frac{1}{\sqrt{2\pi}\lambda} \exp\left[-\frac{(\mathcal{S} - \mathcal{S}_0)^2}{2\lambda^2}\right], \tag{12}$$

where the typical value $\mathcal{S}_0$ is given by Eq. (10) and the width λ increases linearly with $\sqrt{N}$ and W. In Ref. [13], one can find numerical results which are perfectly described by the above analytical expressions when $W = t$.

3 Inelastic thermoelectric transport

When one increases the temperature T, electron transport becomes mainly inelastic and activated. The inelastic effects can be due to electron-electron, electron-photon and electron-phonon interactions. Electron-electron interactions in a many-electron system with localised single-particle states can induce a metal-to-insulator transition above a certain critical temperature [16]. These interactions can also induce the Coulomb-gap behaviour [17] observed in δ-doped $GaAs/Al_xGa_{1-x}As$ 2D heterostructures at low temperature [18], providing evidence of possible phononless hopping. Electron-photon interactions are responsible for the photovoltaic effects. In Ref. [20], we have studied the Variable Range Hopping (VRH) regime introduced by Mott [21] where electron-phonon coupling dominates. Fig.3 (a) illustrates how electrons propagate through the NW in the Mott VRH regime.

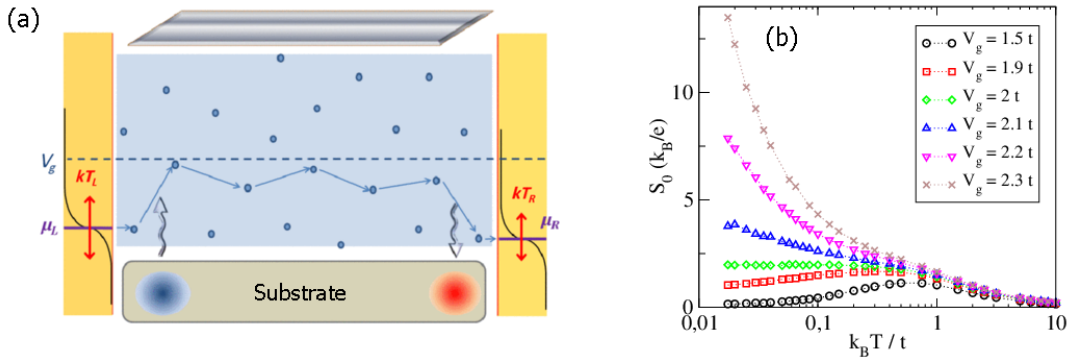

Figure 3: (**a**) The electronic localised states (blue dots) are randomly located along the chain within an energy band of width $4t+W$ (shaded light blue region). In the left and right reservoirs, the electrons are at equilibrium with Fermi-Dirac distributions of temperatures $T_L = T+\delta T$, $T_R = T$ and electrochemical potentials $\mu_L = E_F + \delta\mu$, $\mu_R = E_F$. Varying the voltage V_g applied to the gate (top grey region) shifts the NW conduction band, making possible to probe electron transport inside the band, around its edges or outside the band. The electrons can hop between states of different energies by absorbing or emitting a phonon. For a NW deposited on a substrate, the phonons are provided by the substrate and characterized by a Bose-Einstein distribution of temperature T_S ($T_S = T$ throughout the paper, except in Sec.5). Electrons injected near the lower band edge mainly find available states to jump to at higher energies near the source (left reservoir). This implies that the phonons are mainly absorbed from the substrate near the source (blue region), and emitted back to the substrate near the drain (red region), as indicated by the two arrows. (**b**) Typical thermopower S_0 (in units of k_B/e) as a function of k_BT/t, calculated for a chain of length $L = 200$ ($E_F = 0$ and $W = t$) for increasing values of V_g.

3.1 Variable Range Hopping

In the VRH regime, the electrons propagate by hopping from one localised state of energy E_i to another, of higher energy $E_j > E_i$ by absorbing a phonon or of lower energy $E_j < E_i$ by emitting a phonon. Let us summarize Mott's original argument [21]. The electron transfer from a state i to another state j separated by a distance L_{ij} in space and Δ_{ij} in energy results from a competition between the probability $\propto \exp -(L_{ij}/\xi)$ to tunnel over a length L_{ij} and the probability $\propto \exp -\Delta_{ij}/(k_BT)$ to change the electron energy by an amount $\Delta_{ij} = 1/(\nu L_{ij})$, where ν is the DOS per site. These estimates neglect the energy dependence of ξ and ν around E_F. In 1D, the optimal hopping length is given by the *Mott length* $L_M \simeq (\xi/2\nu k_BT)^{1/2}$, if the localisation lengths ξ and DOS per unit length ν do not vary within the Mott energy window $\Delta_M = 1/(\nu L_M) = k_B\sqrt{TT_M}$ around E_F. L_M decreases as the temperature increases. One defines the activation temperature $k_BT_x \simeq \xi/(2\nu L^2)$ at which $L_M \simeq L$ and the Mott temperature $k_BT_M \simeq 2/(\nu\xi)$ at which $L_M \simeq \xi$. The inelastic VRH regime corresponds to $T_x < T < T_M$ where the electrical conductance

$$G \propto \exp -(2L_M/\xi) \propto \exp -(\Delta_M/k_BT). \tag{13}$$

Below T_x elastic tunneling dominates, while $L_M < \xi$ above T_M and transport becomes simply activated. In 1D, the crossover from VRH to simply activated transport takes even place [22, 23] at a temperature T_a lower than T_M. The reason is the presence of highly resistive regions in energy-position space, where 1D electrons cannot find empty states at distances $\sim \Delta_M, L_M$.

3.2 Random Resistor Network with energy-dependent localisation length and density of states

If the variation of $\xi(E)$ and $\nu(E)$ as a function of the energy E is not negligible within the characteristic scale Δ_M, we need to go beyond this simple argument, notably around the 1D band edges. We use a simplified model where the E_i are N uncorrelated variables of probability given by the DOS $\nu(E)$ of the 1D Anderson model for a chain of length $L = Na$ ($a = 1$), while the N localisation lengths $\xi(E_i)$ are given by the typical values of this model (Eqs. (3) and (4)). The N positions x_i of the localized states are

taken at random in the interval $[0, L]$. As in Refs. [24, 25], we solve the corresponding Miller-Abrahams random resistor network [26] (RRN) made of all possible links connecting the N nodes given by the N localised states. Each pair of nodes i, j is connected by an effective resistor, which depends on the transition rates Γ_{ij}, Γ_{ji} induced by local electron-phonon interactions. For a pair of localised states i and j of energies E_i and E_j, Fermi golden rule [25] gives:

$$\Gamma_{ij} = \gamma_{ij}\, f_i\,(1 - f_j)\,\left[N_{ij} + \theta(E_i - E_j)\right]\,, \tag{14}$$

where f_i is the occupation number of state i and $N_{ij} = [\exp\{|E_j - E_i|/k_BT\} - 1]^{-1}$ is the phonon Bose distribution at energy $|E_j - E_i|$. The Heaviside function accounts for the difference between phonon absorption and emission [19]. γ_{ij} is the hopping probability $i \to j$ due to the absorption/emission of a phonon when i is occupied and j is empty. It is given by

$$\frac{\gamma_{ij}\,(1/\xi_i - 1/\xi_j)^2}{\gamma_{ep}} = \frac{\exp\{-2x_{ij}/\xi_j\}}{\xi_i^2} + \frac{\exp\{-2x_{ij}/\xi_i\}}{\xi_j^2} - \frac{2\exp\{-x_{ij}(1/\xi_i + 1/\xi_j)\}}{\xi_i\xi_j} \tag{15}$$

where $x_{ij} = |x_i - x_j|$ and γ_{ep} depends on the electron-phonon coupling strength and of the phonon density of states. If the energy dependence of ξ and ν can be neglected within Δ_M, one recovers the usual limit $\gamma_{ij} \simeq \gamma_{ep}\exp(-2x_{ij}/\xi)$.

The direct transition rates between each state i and the contacts α (source $\alpha = L$ and drain $\alpha = R$) are assumed to be dominated by elastic tunneling (see Refs. [24, 25]) and read

$$\Gamma_{i\alpha} = \gamma_{e,\alpha}\exp(-2x_{i\alpha}/\xi_i)\, f_i\,\left[1 - f_\alpha(E_i)\right]. \tag{16}$$

$f_\alpha(E) = [\exp\{(E-\mu_\alpha)/k_BT\}+1]^{-1}$ is the contact α's Fermi-Dirac distribution, $x_{i\alpha}$ denotes the distance of the state i from α, and $\gamma_{e,\alpha}$ is a rate quantifying the coupling between the localized states and the contact α. The electric currents flowing between each pair of states and between states and contacts read

$$I_{ij} = e\,(\Gamma_{ij} - \Gamma_{ji}), \tag{17a}$$

$$I_{i\alpha} = e\,(\Gamma_{i\alpha} - \Gamma_{\alpha i}), \qquad \alpha = L, R. \tag{17b}$$

$e < 0$ is the electron charge. Hereafter, we will take $\gamma_{ep} = t/\hbar$ and symmetric couplings $\gamma_{e,L} = \gamma_{e,R} = t/\hbar$.

For solving the RRN, we consider it at equilibrium with a temperature T and a chemical potential $\mu = E_F$ everywhere. A small electric current I_e can be driven by adding to the left contact (the source) a small increase $\delta\mu$ of its chemical potential (Peltier configuration). If $\delta\mu$ is sufficiently small, one has $I_e \propto \delta\mu$ (linear response). At equilibrium ($\delta\mu = 0$), the N occupation numbers f_i are given by Fermi-Dirac distributions $f_i^0 = (\exp[(E_i - E_F)/k_BT] + 1)^{-1}$. When $\mu_L \to E_F + \delta\mu$, $f_i \to f_i^0 + \delta f_i$. For having the currents I_{ij} and $I_{i\alpha}$, we only need to calculate the N changes δf_i induced by $\delta\mu \neq 0$. Imposing current conservation at each node i of the network ($\sum_j I_{ij} + \sum_\alpha I_{i\alpha} = 0$) and neglecting terms $\propto \delta f_i.\delta f_j$ (linear response), one obtained N coupled linear equations. Solving numerically this set of equations gives the N changes δf_i and hence all the currents I_{ij} and $I_{i\alpha}$. From this, we can calculate the total charge $I_L^e = -\sum_i I_{iL}$ and heat $I_{L(R)}^Q = \sum_i (E_i - \mu_{L(R)})/e) I_{iL(R)}$ currents, and hence the electrical conductance G, the Peltier coefficient Π and the Seebeck coefficient S in the VRH regime.

$$G = \frac{I_L^e}{\delta\mu/e}, \quad \Pi = \frac{I_L^Q}{I_L^e}, \quad S = \frac{1}{T}\,\frac{I_L^Q}{I_L^e}. \tag{18}$$

In the last equation, the Kelvin-Onsager relation $\Pi = ST$ has been used for obtaining the thermopower S from the Peltier coefficient Π.

3.3 Activated thermoelectric transport in arrays of parallel NWs

Using the 1D weak-disorder expressions (Eqs. (3)-(5)) for $\nu(E)$ and $\xi(E)$, we have studied activated transport through N localised states of energy E_i and localisation length $\xi(E_i)$. The states were assumed to be randomly located along a chain of length $L = Na$, and the energies E_i were taken at random with a probability $\nu(E)$ inside an energy band $[-2\epsilon, 2\epsilon]$ where $\epsilon = t + W/4$. The corresponding thermopower

distributions $P(S)$ are given and discussed in Ref. [20]. We reproduce in Fig. 3 (**b**) the curves giving the typical thermopower S_0 (in units of k_B/e) as a function of k_BT/t for increasing values of V_g. Taking $E_F = 0$, S_0 has been calculated for a chain of length $L = 200$ with $W = t$. $V_g = 0$ corresponds to the band centre and $V_g/t = \pm 2.5$ to the band edges. When $k_BT < t$, S_0 remains small within the band ($V_g \approx 1.5t$), but becomes much larger around its edges ($V_g = 2.3t$). At higher temperatures, S_0 decreases and becomes independent of V_g. If activated transport at the band edges give rise to large thermopowers, it is also characterized by small electrical conductances, which defavor large values for the power factors Q. This led us to consider in Ref. [27] arrays of parallel nanowires in the field effect transistor device configuration. In such arrays, the conductances add while the thermopower fluctuations self-average. The maximal output power $P_{max} = Q(\delta T)^2/4$ is found to be maximal near the band edges, while the electronic figure of merit (obtained without including the phononic contribution K^{ph} to the thermal conductance) keeps a large value $Z_eT \approx 3$. As estimated in Ref. [27], P_{max} can be of the order of $P_{max} \approx 20\tilde{\gamma}_e \mu W$ for $M = 10^5$ parallel silicon NWs with $\delta T \approx 10K$, $T \approx 100K$, and $t/k_B \approx 150\,\mathrm{K}$. The larger is M or δT, the larger is P_{max}. Estimates of the constant $\tilde{\gamma}_e = \gamma_e \hbar/t$ give values $\approx 0.01 - 1$. If one takes into account K^{ph}, we expect that $ZT \approx Z_eT/(1 + 2/\tilde{\gamma}_e)$ for Silicon suspended NWs, while $ZT \approx Z_eT/(1 + 20/\tilde{\gamma}_e)$ for Silicon NWs deposited on a Silicon Dioxide substrate.

4 Using electron-phonon coupling for managing heat

The phonons have no charge and cannot be manipulated with bias and gate voltages, in contrast to electrons. This makes difficult to manage heat over small scales, unless we take advantage of the electron-phonon coupling for transfering heat from the phonons towards the electrons. Let us show how this can be done using phonon-activated transport near the edges of a NW conduction band. We take a NW deposited on a substrate with a back gate, and assume that the transport of NW-electrons is activated mainly because of the substrate phonons. Let us consider a pair of localised states i and j. The heat current absorbed from (or released to) the substrate phonon bath by an electron hopping from i to j reads $I^Q_{ij} = (E_j - E_i)\, I^N_{ij}$, where $I^N_{ij} = \Gamma_{ij} - \Gamma_{ji}$ is the hopping particle current between i and j. The local heat current associated to the state i is given by summing over the hops from i to all the states j:

$$I^Q_i = \sum_j I^Q_{ij} = \sum_j (E_j - E_i)\, I^N_{ij}. \tag{19}$$

In Fig. 4, we show 2D histograms of the local heat currents I^Q_i as a function of the position x_i of the state i inside the NW. We take the convention that I^Q_i is positive (negative) when the phonons are absorbed (emitted), thus heating (cooling) the electrons at site i. We have numerically solved the random resistor network (see subsection 3.2) for a temperature $k_BT = 0.5t$, $W = t$ and four different values of V_g, corresponding to electron injection at the band center ($V_g = 0$), below the band centre ($V_g = t$) and around the lower ($V_g = 2.25t$) and upper ($V_g = -2.25t$) band edges of the NW conduction band. At the band centre, the fluctuations of the local heat currents are symmetric around a zero average. They are larger near the NW boundaries and remain independent of the coordinate x_i otherwise. Away from the band center, one can see that the fluctuations are no longer symmetric near the NW boundaries, though they become symmetric again far from the boundaries. When the electrons are injected through the NW in the lower energy part of the NW band, more phonons of the substrate are absorbed than emitted near the source electrode. The effect is reversed when the electrons are injected in the higher energy part of the band (by taking a negative gate potential V_g): It is now near the drain that the phonons are mainly absorbed. The 2D histograms corresponding to $V_g = 2.25t$ and $-2.25t$ are symmetric by inversion with respect to $I^Q_i = 0$.

As explained in Refs. [27, 28], activated transport near the band edges of disordered NWs opens interesting ways for managing heat at small scales, notably for cooling hot spots in microprocessors. Taking $M = 2.10^5$ NWs contacting two $1-$cm long electrodes, one estimates that we could transfer $0.15\,\mathrm{mW}$ from the source side towards the drain side by taking $\delta\mu/e \approx 1\,\mathrm{mV}$ at $T = 77\,\mathrm{K}$. Again, the larger is M or $\delta\mu$, the larger is the heat of the substrate which can be transfered from the source towards the drain by hot electrons.

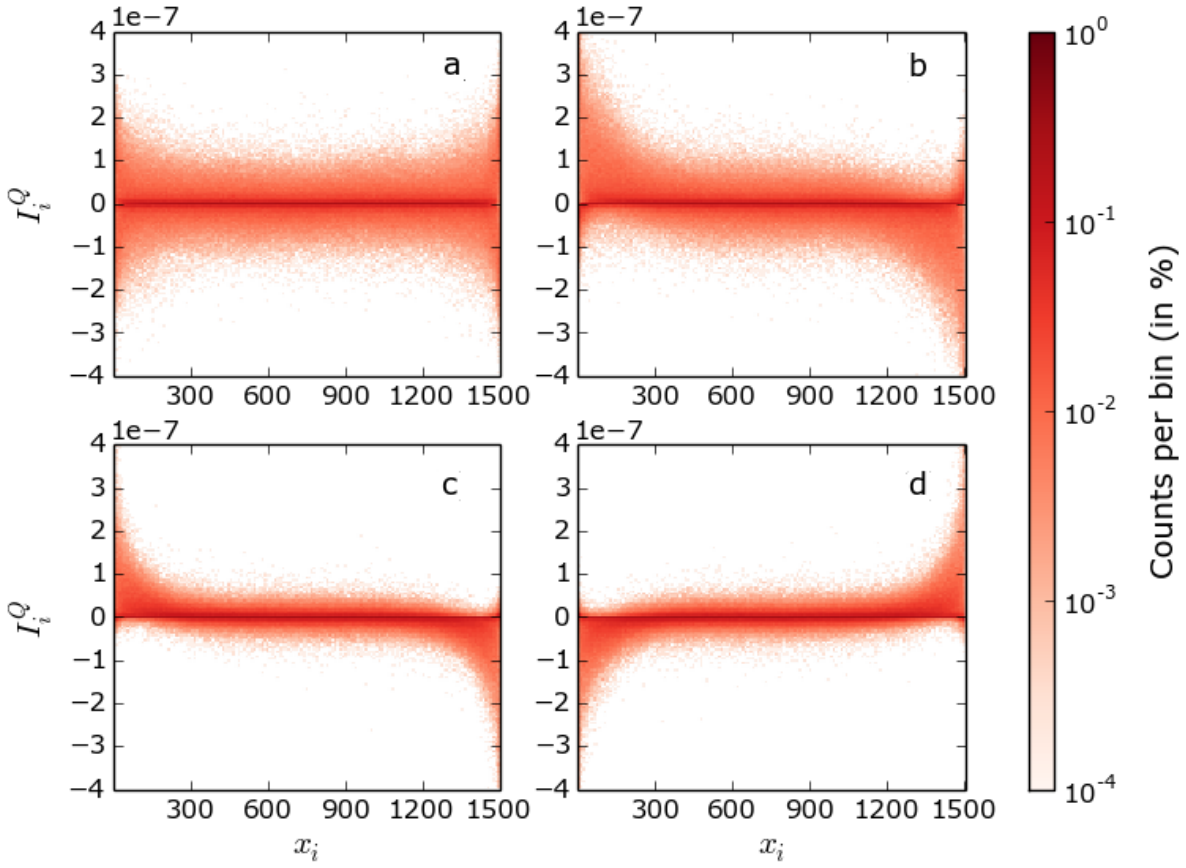

Figure 4: 2D histograms giving the distribution of local heat currents I_i^Q (Eq. (19)) as a function of the position x_i along the NW, for four values of the gate potential: (a) $V_g = 0$, (b) $V_g = t$, (c) $V_g = 2.25t$ and (d) $V_g = -2.25t$. Parameters: $L = 1500$, $W = t$, $k_BT = 0.5t$, $\delta\mu = 10^{-5}t$, statistics over 500 NWs.

5 Activated Multi-terminal thermoelectric transport and Ratchet effects

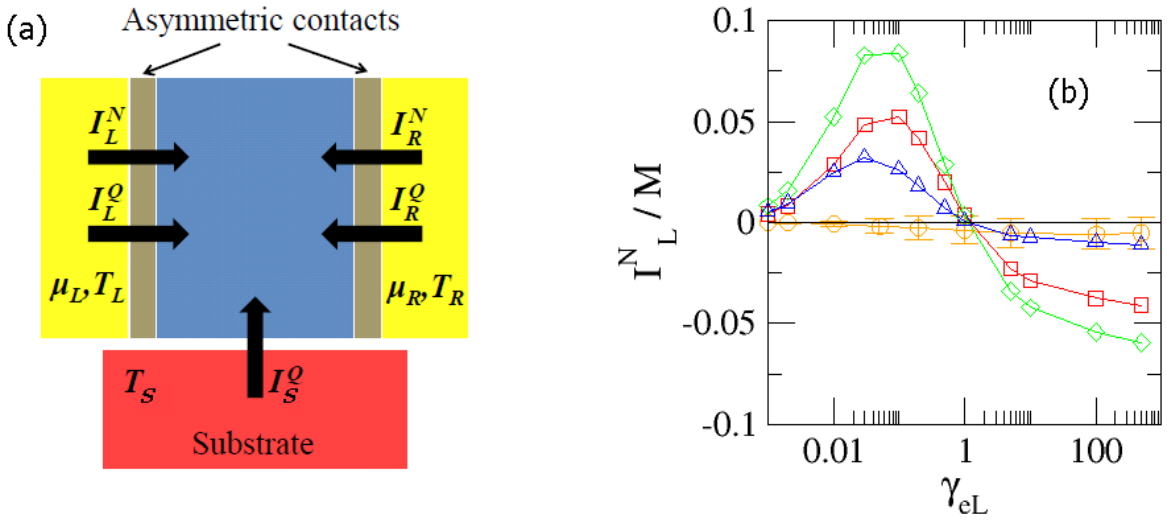

Figure 5: (**a**): Scheme of the three-terminal setup corresponding to activated thermoelectric transport for a NW deposited on a substrate. The NW (blue) is connected to two electronic electrodes (yellow) L (the source) and R (the drain) via asymmetric contacts. The electrodes are at equilibrium (electrochemical potentials μ_L, μ_R, and temperatures T_L, T_R). The insulating substrate (red) provides a phonon bath of temperature T_S. (**b**): Ratchet effect powered by $\delta T_S = 10^{-3}\,\epsilon$ when $\delta T = \delta\mu = 0$. For various values of V_g ($V_g/\epsilon = 0$ (○), 0.5 (□), 1 (◇) and 2.5 (△)), the average particle currents I_L^N/M (in unit of $10^5\epsilon/\hbar$) of an array of $M = 2.10^5$ parallel NWs is given as one varies γ_{eL} (elastic coupling to the source), keeping the same value $\gamma_{eR} = \epsilon/\hbar$ for the elastic coupling to the drain. $I_L^N/M \neq 0$, unless $V_g = 0$ (particle-hole symmetry) or $\gamma_{eL} = \gamma_{eR}$ (inversion symmetry).

In Secs. 3 and 4, we have discussed activated transport in a configuration where the source, drain and substrate were at the same equilibrium temperature T, the heat and particle currents between the source and the drain being induced by a small voltage bias $\delta\mu$ and/or temperature bias δT. More generally, a disordered NW deposited on a substrate can be viewed as the three-terminal setup sketched in Fig. 5 (**a**): Two electronic reservoirs L (source) and R (drain) at equilibrium with electrochemical potentials μ_L, μ_R, and temperatures T_L, T_R, while the substrate provides a third reservoir S of phonons at a temperature T_S. Heat and particles can be exchanged between L and R, but only heat with S. The particle currents I_L^N, I_R^N, and the heat currents I_L^Q, I_R^Q, I_S^Q are taken positive when they enter the NW from the three reservoirs. The drain is chosen as reference ($\mu_R \equiv E_F$ and $T_R \equiv T$) and we set $\delta\mu = \mu_L - \mu_R$, $\delta T = T_L - T_R$, and $\delta T_S = T_S - T_R$. In linear response the charge and heat currents I_L^N, I_L^Q, and the heat current I_S^Q can be expressed à la Onsager in terms of the corresponding driving forces

$$\begin{pmatrix} I_L^N \\ I_L^Q \\ I_S^Q \end{pmatrix} = \begin{pmatrix} L_{11} & L_{12} & L_{13} \\ L_{12} & L_{22} & L_{23} \\ L_{13} & L_{23} & L_{33} \end{pmatrix} \begin{pmatrix} \delta\mu/T \\ \delta T/T^2 \\ \delta T_S/T^2 \end{pmatrix} . \tag{20}$$

The Casimir-Onsager relations $L_{ij} = L_{ji}$ for $i \neq j$ are valid in the absence of time-reversal symmetry breaking. In Ref. [29], we have discussed several possibilities offered by this setup when $\delta T_S \neq 0$, in terms of energy harvesting and cooling. Let us focus on the case where the NW is deposited on a hotter substrate without bias and temperature difference between the source and the drain ($\delta\mu = \delta T = 0$ while $\delta T_S > 0$). If the particle-hole symmetry and the left-right inversion symmetry are broken, the heat provided by the phonons can be exploited to produce electrical work. Let us consider a model where the NW localized states are uniformly distributed in space and energy within a band $[-2\epsilon, 2\epsilon]$

with a constant DOS $\nu = 1/(4\epsilon)$ and an energy independent localisation length $\xi = 4$. We have solved the corresponding RRN for an ensemble of M parallel NWs with asymmetric elastic couplings to the electronics reservoirs. In average over an ensemble of M NWs, particle-hole symmetry is broken if the Fermi potential $E_F \equiv 0$ does not coincide with the NW band centre ($V_g \neq 0$), and inversion symmetry is broken by taking different elastic coupling constants in Eq. (16) ($\gamma_{e,L} \neq \gamma_{e,R}$). Fig. 5 (**b**) gives the average particle current I_L^N/M between the source and the drain as a function of $\gamma_{e,L}$ when $\gamma_{e,R} = 1$ (in units of $\epsilon/\hbar$). I_L^N/M was induced by a temperature difference $\delta T_S = 10^{-3}\epsilon$ between the substrate and a deposited array of $M = 2.10^5$ parallel NWs. One can see that $I_L^N \approx 0$ at the band centre ($V_g = 0$) and when $\gamma_{e,L} = \gamma_{e,R}$, while $I_L^N \neq 0$ otherwise. Other ways of breaking inversion symmetry which give rise to even larger currents I_L^N are discussed in Ref. [29].

6 Conclusion

Our studies were restricted to the elastic tunnel regime and to the Mott VRH regime where electron-phonon interactions dominate. We have considered arrays of parallel purely 1D NWs where the electron states are localised and neglected the effects of electron-electron and electron-photon interactions. In bulk 3D amorphous germanium, silicon, carbon and vanadium oxide [19], the Mott VRH behaviour was observed in a temperature range $60K < T < 300K$. This shows us that Mott VRH is relevant in a broad temperature domain which can reach room temperature. At lower temperatures, Efros-Shklovskii hopping behaviour was observed in 2D heterostructures [18] with a universal prefactor, indicating that the effects of electron-electron interactions become more relevant than these of electron-phonon interactions as one decreases the temperature [30]. Eventually, let us note that in bulk weakly-doped crystalline semiconductors, the electrons can be activated from the impurity band up to the conduction band when the temperature exceeds the energy gap between these two bands, putting an upper limit to VRH transport. The width of this energy gap can vary from one material to another. This is what can be said for bulk 3D or 2D materials. To extend these conclusions to 1D NWs is not straightforward, since the effect of disorder (Anderson localisation) and of electron-electron interactions (Wigner glass) are much more relevant in the 1D limit. Moreover, the temperature range where our predictions apply can vary from one semiconductor to another, and can depend on the width of the NWs.

In summary, we have shown that arrays of 1D MOSFETs have good thermoelectric performances, notably when the electrochemical potential is in the vicinity of the NW band edges. The described effects could provide an interesting method for converting waste heat into useful electrical power and for cooling hot spots in microprocessors. Ratchet effects open interesting perspectives when electrical transport in deposited NWs can be activated by the phonons of the substrate. The studied devices are based on standard nanofabrication technologies which are widely developed in semiconductor microelectronics.

References

[1] E. Pop, S. Sinha and K. Goodson, Heat Generation and Transport in Nanometer-Scale Transistors, Proceedings of the IEEE. 94 (2006) 1587. DOI: 10.1109/jPROC.2006.879794

[2] A. F. Ioffe, Semiconductor thermoelements, and thermoelectric cooling, Infosearch Limited, 1957.

[3] H. J. Goldsmid, Introduction to thermoelectricity, Springer-Verlag, 2010.

[4] A. I. Hochbaum, R. Chen, R. D. Delgado, W. Liang, E. C. Garnett, M. Najarian, A. Majumdar and P. Yang, Enhanced thermoelectric performance of rough silicon nanowires, Nature, 451, (2008) 163. DOI: 10.1038/nature06381.

[5] W. Poirier, D. Mailly and M. Sanquer, Tunneling and interferences in very small GaAs metal-semiconductor field-effect transistors, Phys. Rev B 59, 16 (1999) 10 856.

[6] C. Thelander, P. Agarwal, S. Brongersma, J. Eymery, L. F. Feiner, A. Forchel, M. Scheffler, W. Riess, B. J. Ohlsson, U. Gsele and L. Samuelson, Nanowire Based One-Dimensional Electronics. MaterialsToday 9 (10) (2006) 28-35.

[7] A. I. Boukai, Y. Bunimovich, J. Tahir-Kheli, W. A. Goddard III and J. R. Heath, Silicon nanowires as efficient thermoelectric materials. Nature,Vol 451 — 10 (2008) 168. doi:10.1038/nature06458.

[8] X. Sun, Z. Zhang and M. S. Dresselhaus, Theoretical modeling of thermoelectricity in BI nanowires. Appl. Phys. Lett. 74, 4005 (1999); doi: 10.1063/1.123242.

[9] N. Mingo, Thermoelectric figure of merit and maximum power factor in III-V semiconductor nanowires. Appl. Phys. Lett. 84, 2652 (2004); doi; 10.1063/1.1695629.

[10] C.-H. Lee, G.-C. Yi, Y. Zuev and P. Kim, Thermoelectric power measurements of wide band gap semiconducting nanowires. Appl. Phys. Lett. 94, 022106 (2009); doi: 1063/1.3067868.

[11] Y.-M. Lin, X. Sun and M. S. Dresselhaus, Theoretical investigation of thermoelectric transport properties of cylindrical Bi nanowires. Phys. Rev. B 62, 7, 4610 (2000).

[12] Y. U. Brovman, J. P. Small, Y. Hu, Y. Fang, C. M. Lieber and P. Kim, Electric field effect thermoelectric transport in individual silicon and germanium/silicon nanowires, J. Appl. Phys. 119 (2016) 234304. DOI: 10.1063/1.4953818.

[13] R. Bosisio, G. Fleury and J.-L. Pichard, Gate-modulated thermopower in disordered nanowires: I. Low temperature coherent regime, New J. Phys. 16 (2014) 035004. DOI: 10.1088/1367-2630/16/3/035004.

[14] B. Derrida and E. Gardner, Lyapunov exponent of the one dimensional Anderson model: weak disorder expansion. J. Phys. France 45 (1984) 1283.

[15] S. A. van Langen, P. G. Silvestrov and C. W. J. Beenakker, Thermopower of single-channel disordered and chaotic conductors, Supperlattices and Microstructures, 23 (1998) 691.

[16] D. M. Basko, I. L. Aleiner and B. L. Altshuler, Metal-insulator transition in weakly interacting many-electron system with localized single-particle states. Annals of Physics321 (2006) 1126; doi:10.1016/j.aop.2005.11.014.

[17] B. I. Shklovskii and A. L. Efros, Electronic Properties of Doped Semiconductors (Springer, Berlin 1984).

[18] S. I. Khondaker, I. S. Shlimak, J. T. Nicholls, M. Pepper and D. A. Ritchie, Two-dimensional hopping conductivity in δ-doped $GaAs/Al_xGa_{1-x}As$ heterostructure. Phys. Rev. B 59, 7 (1999) 4580.

[19] V. Ambegaokar, B. I. Halperin and J. S. Langer, Hopping conductivity in disordered systems, Phys. Rev. B 4, 8 (1970) 2612.

[20] R. Bosisio, C. Gorini, G. Fleury and J.-L. Pichard, Gate-modulated thermopower in disordered nanowires: II. Variable-range hopping regime, New J. Phys. 16, (2014) 095005. DOI: 10.1088/1367-2630/16/9/095005

[21] N. F. Mott and E. A. Davies, Electronic Processes in Non Crystalline Materials, 2nd edn (1979) (Oxford: Clarendon).

[22] J. Kurkijarvi, Hopping conductivity in one dimension, Phys. Rev B 8 (1973) 922.

[23] M. E. Raikh and M. E. Ruzin, Fluctuations of the hopping conductance in one dimensional systems, Sov. Phys. JETP 68 (1989) 642.

[24] J. H. Yiang, O. Entin-Wohlman and Y. Imry, Thermoelectric three-terminal hopping transport through one-dimensional nanosystems, Phys. Rev. B 85 (2012) 075412.

[25] J. H. Yiang, O. Entin-Wohlman and Y. Imry, Hopping thermoelectric transport in finite systems: Boundary effects, Phys. Rev. B 87 (2013) 205420.

[26] A. Miller and E. Abrahams, Impurity conduction at low concentrations Phys. Rev. 120 (1960) 745.

[27] R. Bosisio, C. Gorini, G. Fleury and J.-L. Pichard, Using Activated Transport for Energy Harvesting and Hot-Spot Cooling, Phys. Rev. Applied 3 (2015) 054002. DOI: 10.1103/PhysRevApplied.3.054002

[28] R. Bosisio, C. Gorini, G. Fleury and J.-L. Pichard, Absorbing/emitting phonons with one dimensional MOSFETs, Physica E, 74 (2015) 340.
DOI: 10.1016/j.physe2015.07012

[29] R. Bosisio, G. Fleury, J.-L. Pichard and C. Gorini, Nanowire-based thermoelectric ratchet in the hopping regime, Phys. Rev. B 93, (2016) 165404. DOI: 10.1103/PhysRevB.93.165404

[30] L. Fleishman, D. C. Licciardello, and P. W. Anderson, Elementary Excitations in the Fermi Glass, Phys. Rev. Lett. 40 (1978) 1340. DOI: 10.1103/PhysRevLett.40.1340